

The Stellar Dynamics of M87

David Merritt

Department of Physics and Astronomy, Rutgers University, New Brunswick, NJ 08855

Siang Peng Oh

Princeton University Observatory, Princeton, NJ 08544

Rutgers Astrophysics Preprint Series No. 195

ABSTRACT

We extract the shape of the stellar velocity ellipsoid as a function of radius in M87 from van der Marel's (1994) velocity dispersion data. We include the gravitational force of a central black hole with the mass quoted by Harms et al. (1994). The kinematical data are corrected for the effects of seeing and instrumental blurring using a nonparametric algorithm. We find that the stellar motions in M87 are slightly radially anisotropic throughout the main body of the galaxy, with $\sigma_r \approx 1.2\sigma_t$. However σ_t *exceeds* σ_r within the inner $1'' - 2''$ by a statistically significant amount. A number of models for the formation of nuclear black holes predict a tangential anisotropy in the stellar motions, and our results provide evidence for such an effect in M87.

1. Introduction

Possibly no elliptical galaxy has been as thoroughly studied as M87 (NGC 4486) in the Virgo cluster. Early observations of the core of M87 revealed a velocity dispersion profile that rose toward the center, a feature that was initially attributed to the presence of a massive ($\sim 5 \times 10^9 M_\odot$) black hole (Sargent et al. 1978). The same data were soon interpreted in other ways; for instance, Binney & Mamon (1982) demonstrated that models without a central point mass were equally acceptable if one was willing to let the stellar velocity ellipsoid become strongly prolate at ~ 100 pc from the center. Such extreme models were later shown to be dynamically unstable (Merritt 1987), but the instability led only to the formation of a mildly elongated bar, which – if viewed from a line-of-sight not far from its major axis – yielded nearly the same dependence of velocity dispersion on radius as the anisotropic spherical model. The most recent, stellar kinematical data (Dressler & Richstone 1990; Jarvis & Peletier 1991; van der Marel 1994) reveal that the

velocity dispersion fails to rise within the inner few arc seconds of M87. These data require even less anisotropy than the earlier, black-hole-free models. In fact, as emphasized by Dressler & Richstone (1990), a $\sim 4 \times 10^9 M_\odot$ black hole can only be reconciled with the velocity dispersion data if one assumes that the stellar motions near the center of M87 are nearly *circular*, a configuration that they found implausible. The stellar dynamical data thus seem to provide little if any evidence for a dark central mass.

The case for a massive black hole in M87 is nevertheless quite strong. Ford et al. (1994) and Harms et al. (1994) discovered a rapidly-rotating, ionized gas disk within the inner arc second of M87, with a major axis roughly perpendicular to the M87 jet. At a radius of $\pm 0.22'' = 16$ pc along the major axis of the disk, the spectra show emission lines separated by $2V = 916$ km s $^{-1}$. If this gas is in approximately circular motion, and if the disk is inclined at 42° as implied by the apparent axial ratio, then M87 contains a central dark mass of $M_h \approx 2.4 \times 10^9 M_\odot$ (Harms et al. 1994). More recent HST observations at higher spatial resolution (Ford et al. 1996) appear to confirm this result.

A nuclear black hole with this mass would be expected to affect the stellar motions within a radius $r_h = GM_h/\sigma^2 \approx 80$ pc $\approx 1''$ in M87, where $\sigma \approx 400$ km s $^{-1}$ is the stellar velocity dispersion. (We assume throughout a distance to M87 of 16 Mpc; thus $1''$ corresponds to 77.6 pc.) However no increase in the stellar velocities is seen in the inner few arc seconds; in fact the best ground-based data suggest a slight *decrease* in the velocity dispersion inside $1'' - 2''$ (e.g. Fig. 1 of Jarvis & Peletier 1991).

These apparently contradictory data can be reconciled if the stellar motions are appreciably circular within the radius of influence of the black hole. Such a model will not keep the observed velocity dispersions low at arbitrarily small radii – orbital velocities sufficiently close to the black hole must eventually rise according to Kepler’s law – but a local bias toward circular motions at $r \approx r_h$ can reduce the line-of-sight dispersions at $\sim 1''$ by an amount that is sufficient to reproduce the stellar velocity dispersion measurements (Dressler & Richstone 1990). It is interesting that a number of models for the formation of massive black holes predict anisotropy in the stellar motions at radii close to GM_h/σ^2 . For instance, the adiabatic growth of a black hole in a pre-existing galaxy core always produces a slight enhancement of circular motions at the expense of radial ones (Goodman & Binney 1984). An even stronger effect may be predicted by models in which black holes form by the coalescence of smaller black holes (Ebisuzaki, Makino & Okumura 1991); here the anisotropy results from the ejection of stars on elongated orbits due to three-body scattering by the black hole binary (Quinlan 1996).

In the present paper, we re-analyze the van der Marel (1994) velocity dispersion data, assuming the presence of a nuclear black hole with the mass quoted by Harms et al.

(1994). We make use of the fact that – in a spherical system with a known gravitational potential – the shape of the stellar velocity ellipsoid at every radius follows uniquely from the observed velocity dispersion profile (Binney & Mamon 1982). In the case of M87, the stellar M/L (e. g. Richstone & Tremaine 1985) implies that the black hole dominates the gravitational force out to a radius of $\sim 250 \text{ pc} \approx 3''$. The stars also contribute to the gravitational force, of course, but their contribution can be reasonably approximated by assuming a constant mass-to-light ratio; M/L can then be derived from the virial theorem independent of any assumptions about the velocity anisotropy. Such a model is likely to be only approximately correct at large radii, where the dark matter surrounding M87 begins to affect the gravitational potential. But it is probably an excellent approximation at small radii where the influence of the black hole on the motions of the stars is significant.

The same conceptual model has been used in many previous studies of the stellar dynamics of M87. Our treatment is new, however, in two ways. First, ours is the first study to make use of the black hole mass as determined by Harms et al. (1994) and Ford et al. (1996). Thus we are able to specify a definite value for M_h (although we consider also the effect of varying M_h by its estimated uncertainty). Second, our treatment of the data is more sophisticated than in previous studies. Since the dependence of the velocity anisotropy on radius, $\beta(r) = 1 - \sigma_t^2(r)/\sigma_r^2(r)$, is not known a priori, the goal should be to generate an estimate of this function directly from the data. In other words, one should approach the estimation of $\beta(r)$ as an inverse problem, not as a model-fitting problem. Binney & Mamon (1982) attempted to infer $\beta(r)$ directly from the data that were available at the time, but they chose to represent the velocity dispersion profile using an ad-hoc set of template curves, thus weakening the model-independence of their results. Binney & Mamon also did not take into account the possible effects of seeing and instrumental blurring on the velocity dispersion data. Van der Marel (1994) took the opposite, “model-fitting” approach, assuming a parametrized functional form for $\beta(r)$ and then predicting how a given model would appear after projection into observable space. However he did not consider any functional forms for $\beta(r)$ in which the stellar motions were circularly biased at small radii, as predicted by the black-hole formation models discussed above.

The algorithm presented here combines the best features of both these studies. We ask simply: What smooth functions $\beta(r)$ are consistent with the measured set of velocity dispersions? This is an ill-posed problem, since many functional forms for $\beta(r)$ are likely to be consistent with the data after projection through the galaxy and after blurring by the atmosphere and the detector. We accordingly use a regularized algorithm to find the “most likely” expression for $\beta(r)$. The uncertainty in our estimate is itself estimated via a standard bootstrap algorithm; the ill-conditioning of the inverse problem manifests itself most strongly as a widening of the confidence bands at small and large radii, where the data

do not strongly constrain the solutions. At no point do we make any assumptions about the functional forms of the observed profiles or of $\beta(r)$, except insofar as we require these functions to be continuous and smooth. Thus we achieve the model-independence aspired to by Binney & Mamon (1982), while fully accounting for observational degradation of the data as in van der Marel (1994).

We find that a black hole with the mass determined by Harms et al. (1994) and Ford et al. (1996) implies a substantial change in the shapes of the stellar orbits near the center of M87. In order to reproduce the low, central value of the velocity dispersion, the stellar orbits must become appreciably circular within the radius of influence of the black hole. The statistical significance of this result depends somewhat on the exact value assigned to M_h ; the larger M_h , the greater the tangential anisotropy implied by the velocity dispersion data. Such a result – although superficially implausible for a hot stellar system – deserves to be taken seriously in the light of black-hole formation models that predict a circular bias in the stellar orbits at $r \approx r_h$.

The data, none of which are new, are summarized in §2. The nonparametric algorithm used to correct the velocity dispersion data for seeing and for instrumental blurring is presented in §3. The derivation of $\beta(r)$ is the subject of §4, and in §5 we interpret our results in the light of recent models for the formation of nuclear black holes.

2. Data

Only two observational quantities are needed for this study: the surface brightness profile of the starlight in M87, $\Sigma(R)$; and the line-of-sight velocity dispersion profile of the stars, $\sigma_p(R)$. (We assume throughout that M87 is spherically symmetric.) The published sources from which our data were derived are as follows.

HST I-band photometry of M87 for $R < 20''$ were presented by Lauer et al. (1992). These data have an estimated spatial resolution of $\sim 0.1''$. Between $20''$ and $163''$, ground-based, R_c band photometry of M87 was published by Peletier et al. (1990). We converted the latter data to I-band via $R_c - I = 1.153$, the average color at these radii. The surface brightnesses were then corrected for galactic extinction using $A_I = 0.04$ (van der Marel 1994).

Our velocity dispersion data were taken from van der Marel (1994), who used the 4.2m William Herschel Telescope in subarcsecond seeing to obtain high S/N spectra of M87 within $\sim 25''$. We followed van der Marel’s practice of using only the G-band data presented in his

Table C1. Measurements of σ_p at positive and negative radii were averaged and their quoted errors reduced using standard formulae for error propagation. These data are presented in Fig. 1.

3. Correction of the Data for Seeing and Instrumental Blurring

The data consist of a set of measurements d_i at discrete positions R_i and their estimated errors ϵ_i . Our goal is to extract smooth representations of functions like $\beta(r)$ from these (noisy and incomplete) data. The relation between the data and the unknown function (call it u) has the implicit form

$$d_i = \mathcal{L}_i u + e_i \tag{1}$$

where \mathcal{L}_i is a linear operator relating u to measured quantities at $R = R_i$, and e_i represents scatter of the data around their mean value at R_i , due in part to measurement errors.

The operator \mathcal{L} contains contributions from two sorts of effects: data degradation due to instrumental limitations, seeing, binning, etc; and projection of the intrinsic function u into observable space – for instance, projection onto the plane of the sky. To the extent that both effects are understood, at least in a statistical sense, we can write an expression for \mathcal{L} and apply regularized inversion algorithms to solve for the most likely u (Merritt 1993a). Confidence bands on the function estimates can then be computed via the bootstrap (Efron 1982). The regularization is necessary since the inverse operation \mathcal{L}^{-1} is typically ill-conditioned (O’Sullivan 1986), so that direct inversion of the data would produce unacceptably noisy results.

Rather than derive a single expression for \mathcal{L} that includes all of the relevant effects, we chose first to correct the data for seeing and instrumental blurring, and then to operate directly on the resulting smooth profiles via the inverse operator \mathcal{L}^{-1} that represents spatial deprojection alone. This two-step procedure is perfectly justified from a statistical point of view (e.g. Wahba 1990, p. 19) and has the advantage that it allows us to separate the effects of instrumental blurring from the effects of spatial deprojection.

The spatial resolution of the Lauer et al. (1992) HST surface photometry, $\sim 0.1''$, is much greater than that of the velocity dispersion observations in the region $R < 20''$ where the two data sets overlap. We can therefore ignore instrumental blurring in our estimate of the stellar luminosity density profile $\nu(r)$. We derived a nonparametric estimate of $\Sigma(R)$ by fitting a smoothing spline (Wahba 1990) to the logarithms of the photometric data, $\log \Sigma_i$

vs. $\log R_i$. The smoothing parameter was chosen by generalized cross-validation (Wahba 1990, p. 52). This estimate was then substituted into Abel’s equation,

$$\nu(r) = -\frac{1}{\pi} \int_r^\infty \frac{d\Sigma}{dR} \frac{dR}{\sqrt{R^2 - r^2}}, \quad (2)$$

to yield an estimate of $\nu(r)$. The result was found to be almost indistinguishable from the profile displayed by van der Marel (1994, Fig. 8), who used the same photometric data as us. We therefore do not reproduce our estimate of $\nu(r)$ here. We note in passing that M87 – although still often described as having a “core” (e.g. Kormendy & Richstone 1995) – in fact has a luminosity density profile that increases as a nearly-perfect power law at small radii, $\nu \sim r^{-1}$, $r < 100$ pc. This profile appears superficially core-like since an $\sim r^{-1}$ density profile produces only a logarithmic divergence when seen in projection.

In the case of the velocity dispersion measurements, which were made from the ground, the observed values might be strongly affected near the galaxy center by atmospheric seeing and by the finite spatial resolution of the detector. Here we generate, from the observed velocity dispersions $\sigma'_p(R_i)$, an estimate of the true velocity dispersion profile $\sigma_p(R)$ that would have been observed using a perfect detector in the absence of atmospheric blurring. This estimate will be used in the next section to generate estimates of the anisotropy profile.

The true velocity dispersion profile $\sigma_p(R)$ is related to the observed profile $\sigma'_p(R)$ via

$$\Sigma'(R)\sigma_p'^2(R) = \frac{1}{4lw} \int_{-\infty}^{\infty} dX \int_{-\infty}^{\infty} dY \Sigma(\sqrt{X^2 + Y^2}) \sigma_p^2(\sqrt{X^2 + Y^2}) \times \int_{R-l}^{R+l} dx \int_{-w}^w dy \text{PSF} \left[\sqrt{(X-x)^2 + (Y-y)^2} \right] \quad (3)$$

(e.g. Qian et al. 1995). Here PSF is the atmospheric point spread function; we adopt van der Marel’s (1994) expression:

$$\text{PSF}(R) = A_1 e^{-R^2/2\sigma_1^2} + A_2 e^{-R^2/2\sigma_2^2}, \quad (4)$$

with $\sigma_1 = 0.313''$, $\sigma_2 = 0.751''$, $A_1 = 0.929$, and $A_2 = 0.121$. The inner integration is over the rectangle whose x -dimension $2l$ is the CCD pixel width, and whose y -dimension $2w$ is the slit width. These values were taken from Tables 1 and C1 of van der Marel (1994); beyond $3''$ from the center, data from more than one pixel were binned together, making l a function of position. The outer integration is over the 2-D image of the galaxy, assumed to be spherically symmetric. Finally, $\Sigma'(R)$ is the surface brightness profile as it would appear after convolution with the seeing disk and the detector.

Interchanging the order of integration, we can write

$$\Sigma'(R)\sigma_p'^2(R) = \sum_{k=1,2} \int_0^\infty dR' \Sigma(R')\sigma_p^2(R') \int_0^{2\pi} d\theta K_i(R, R', \theta), \quad (5)$$

$$K_k(R, R', \theta) = \frac{A_k \pi \sigma_k^2}{8lw} \left[\operatorname{erf} \left(\frac{R' \cos \theta - R + l}{\sqrt{2}\sigma_k} \right) - \operatorname{erf} \left(\frac{R' \cos \theta - R - l}{\sqrt{2}\sigma_k} \right) \right] \times \left[\operatorname{erf} \left(\frac{R' \sin \theta + w}{\sqrt{2}\sigma_k} \right) - \operatorname{erf} \left(\frac{R' \sin \theta - w}{\sqrt{2}\sigma_k} \right) \right] \quad (6)$$

where $X = R' \cos \theta$ and $Y = R' \sin \theta$. This relation can be discretized by writing $g_i = \Sigma'(R_i) \sigma_p^{2'}(R_i)$ and $h_j = \Sigma(R_j) \sigma_p^2(R_j)$, where R_i and R_j are radial grid values. We then have

$$g_i \approx \sum_{j=1}^{n-1} A_{ij} h_j, \quad (7)$$

with

$$A_{ij} = \int_{R'_j}^{R'_{j+1}} dR' \int_0^{2\pi} d\theta K(R_i, R', \theta). \quad (8)$$

This is a “product integration” scheme, and the desired function h is obtained by inverting Eq. (7); h_j is identified with the solution value at the midpoint of the interval (R_j, R_{j+1}) .

One could attempt to invert Eq. (7) directly, but the result would be unacceptably noisy due to the ill-conditioning of the matrix \mathbf{A} . (We in fact attempted direct inversion, with discouraging results.) Instead, we looked for the roughness-penalized function \hat{h}_j that minimizes

$$\sum_i \left(g_i - \sum_j A_{ij} h_j \right)^2 + \lambda \int \left(\frac{d^2 \log \sigma_p}{dR^2} \right)^2 dR \quad (9)$$

for some appropriately-chosen λ , the smoothing parameter. We represented the penalty function discretely as well, via the approximation

$$\lambda \sum_j (R_{j+1} - R_j) \left[\frac{\sigma_{p_{j+1}} - 2\sigma_{p_j} + \sigma_{p_{j-1}}}{(R_{j+1} - R_j)^2} \right]^2. \quad (10)$$

The selection of the optimal smoothing parameter in ill-conditioned problems is, itself, an ill-conditioned problem (Wahba 1990, p. 105). An “infinitely smooth” estimate, i.e. the limiting estimate for large λ , would be exponential in our case, $\log \sigma_p \propto R$. We estimated the optimal λ by eye. Appreciably smaller values led to estimates that seemed unphysically noisy, while much larger values biased the solution toward the infinitely smooth, exponential dependence. For a fairly wide range of λ 's around our adopted value, however, there was no significant variation in the form of the estimated function.

The results are shown in Fig. 1. The solid curve is our estimate of the corrected, line-of-sight velocity dispersion profile, $\hat{\sigma}_p(R) = \sqrt{\hat{h}(R)/\Sigma(R)}$. The dashed lines in Fig. 1 are confidence bands on the estimate. These were constructed by first generating 300

bootstrap data sets $\tilde{\sigma}_p(R_i)$ from the original data, according to the scheme:

$$\tilde{\sigma}_p(R_i) = f(R_i) + \delta_i, \quad (11)$$

where f is a smoothing spline fit to the uncorrected data and $\delta_i \sim \mathcal{N}(0, \epsilon_i)$ is a random number generated from the normal distribution with dispersion equal to the measurement error at R_i (Wahba 1990, p. 71). For each of these bootstrap samples, the deblurring algorithm just defined was used to estimate $\sigma_p(R)$. The distribution of bootstrap estimates at every R was then used to construct the confidence bands in the figure.

The corrected velocity dispersion profile in Fig. 1 follows the raw data outside of $\sim 1''$. At smaller radii, the corrected profile rises slightly above the mean relation defined by the measured values. We would not expect the corrected profile to deviate strongly from the raw data even at these small radii, since the observed velocity dispersions are approximately constant within the inner two arc seconds, and a flat profile remains flat after deblurring. However, the bootstrap confidence bands suggest that quite a wide range of profile shapes are consistent with the data inside of $\sim 1''$, from a flat or inwardly decreasing profile, to one that increases as far as $\sim 450 \text{ km s}^{-1}$ at $0.1''$ (95%). We note that the widening of the confidence bands at small radii is due primarily to the amplification of errors that accompanies the deconvolution; the measurement errors quoted by van der Marel (1994) are almost independent of radius, but their consequences become greater near the center due to the increased importance of the seeing and instrumental corrections there.

The flatness of the velocity dispersion profile very near the center of M87 was noted by Dressler (1980), Dressler & Richstone (1990), Jarvis & Peletier (1991) and van der Marel (1994) in their respective data sets. This result appears therefore to be robust, although it could of course reflect some systematic error in the interpretation of the data. Dressler & Richstone (1990) emphasized the difficulty of reconciling a low central velocity dispersion with a massive ($M_h > 10^9 M_\odot$) nuclear black hole, unless the stellar motions become strongly anisotropic near the center. We will confirm their result below.

4. Estimation of the Velocity Anisotropy

In a nonrotating, spherical stellar system, the dependence of the velocity anisotropy $\beta = 1 - \sigma_t^2/\sigma_r^2$ on radius can be inferred uniquely from the observed velocity dispersion profile $\sigma_p(R)$, if one is willing to assume that the functional form of the gravitational potential is known (Binney & Mamon 1982). We assume that the gravitational potential of M87 can be expressed as

$$\Phi(r) = -\frac{GM_h}{r} + \left(\frac{M}{L}\right) \Phi_L(r), \quad (12)$$

where M_h is the mass of the central black hole, M/L is the mass-to-light ratio of the stars, and Φ_L is the “potential” corresponding to the stellar luminosity distribution:

$$\Phi_L(r) = -4\pi G \left(\frac{1}{r} \int_0^r \nu r^2 dr + \int_r^\infty \nu r dr \right), \quad (13)$$

with $\nu(r)$ the luminosity density. The expression (12) is not completely general, since it assumes that the stellar mass-to-light ratio is independent of radius. However we expect Eq. (12) to be sufficiently general out to a radius of several arc seconds where the black hole dominates the gravitational force. Relaxing the assumption of a constant M/L would make the derivation of $\beta(r)$ impossible without additional kinematical information (Merritt 1993b).

The stellar velocity dispersion in the radial direction is given by

$$\nu(r)\sigma_r^2(r) = - \frac{2}{\pi r^3} \int_r^\infty \left[\frac{r}{\sqrt{R^2 - r^2}} + \cos^{-1} \left(\frac{r}{R} \right) \right] \Sigma(R)\sigma_p^2(R) R dR \quad (14)$$

$$+ \frac{2}{3r^3} \int_r^\infty \left(r'^3 + \frac{1}{2}r'^3 \right) \nu(r') \frac{d\Phi}{dr'} dr' \quad (15)$$

(Dejonghe & Merritt 1992, Eq. 57a), and the tangential component follows from the spherical Jeans equation:

$$\sigma_t^2 = \sigma_r^2 + \frac{r}{2} \left(\frac{d\Phi}{dr} + \frac{1}{\nu} \frac{d\nu\sigma_r^2}{dr} \right). \quad (16)$$

We can obtain a nonparametric estimate of $\sigma_r(r)$ by substituting our smooth estimates of $\nu(r)$, $\Sigma(R)$ and $\sigma_p(R)$ into Eq. (15) (Wahba 1990, p. 19). However we first need to specify the parameters M_h and M/L that appear in our expression (12) for the potential.

We first consider M_h . Ford et al. (1994) used HST WFPC-2 narrow-band images of M87 to find a 100 pc ($\sim 1''$) scale disk of ionized gas with a major axis oriented approximately perpendicular to the M87 jet. Harms et al. (1994) used COSTAR and the FOS to measure the velocity at five positions in this disk and concluded that there was Keplerian rotation around a mass of $(2.4 \pm 0.7) \times 10^9 M_\odot$. More recent HST observations with a smaller, 0.086'' aperture appear to confirm this interpretation, although the scatter in the velocities is still consistent with a fairly wide range of masses, from 1 to $3.5 \times 10^9 M_\odot$ (Ford et al. 1996). This range is essentially equal to the $\pm 2\sigma$ interval quoted by Harms et al. (1994). We will accordingly compute our kinematical solutions using the three values $M_h = \{1.0, 2.4, 3.8\} \times 10^9 M_\odot$, corresponding to the Harms et al. (1994) value plus or minus twice its estimated uncertainty.

The second parameter, M/L , can be derived from the observed velocity dispersion profile independent of any assumptions about the stellar velocity anisotropy. The virial

theorem

$$3 \int_0^\infty \Sigma \sigma_p^2 R \, dR = 2 \int_0^\infty \nu \frac{d\Phi}{dr} r^3 \, dr \quad (17)$$

(e. g. Dejonghe & Merritt 1992, Eq. 51) becomes, with our assumed form for $\Phi(r)$,

$$\frac{M}{L} = \frac{3 \int_0^\infty dR \, R \Sigma \sigma_p^2 - 2GM_h \int_0^\infty dr \, r \nu}{8\pi G \int_0^\infty dr \, r \nu \int_0^r dr' r'^2 \nu}, \quad (18)$$

which allows M/L to be determined from previously-computed quantities. (In order to evaluate the integrals in Eqs. (15) and (18) that extend to infinite radius, the velocity dispersion profile was extrapolated as a power law beyond $25''$.) Our estimates of the I-band M/L in solar units are given in Table 1. Finally, confidence bands on M/L and on the function estimates were generated by repeating the set of computations just described for each of the 300, bootstrap-generated data sets defined above.

Estimates of $\sigma_r(r)$, $\sigma_t(r)$ and $\beta(r)$ and their 95% confidence bands are shown in Fig. 2. Fig. 2b gives results for $M_h = 2.4 \times 10^9 M_\odot$, the value preferred by Harms et al. (1994), while Figs. 2a and 2c illustrate how these function estimates change when M_h is increased or decreased by twice its estimated uncertainty of $0.7 \times 10^9 M_\odot$. The confidence bands become very wide at both large and small radii. At small radii, the effects of spatial deprojection and instrumental deblurring are greatest. At large radii, the lack of velocity data beyond $\sim 25''$ implies a large variance in quantities like σ_r that formally depend on integrations to infinity.

For $M_h = 1.0 \times 10^9 M_\odot$, $\beta(r)$ is found to remain approximately constant with radius, $\beta(r) \approx 0.4 - 0.5$, corresponding to $\sigma_r/\sigma_t \approx 1.3\sigma_t$. The stellar velocity ellipsoid is radially elongated everywhere in this case, although the 95% confidence bands are consistent with motions that are close to isotropic. The need for radially-biased motions when the black hole mass is small or zero has been noted by a number of authors including Binney & Mamon (1982), Dressler & Richstone (1990), and van der Marel (1994).

However when M_h is increased to its preferred value of $2.4 \times 10^9 M_\odot$, $\beta(r)$ is forced to decline at small radii in order to maintain the observed, low value of the central velocity dispersion. The central decline in $\beta(r)$ becomes even more extreme if M_h is increased to $3.8 \times 10^9 M_\odot$ – in this case, the inferred value of σ_r^2 actually falls below zero inside of $\sim 0.4''$ (Fig. 2c). A similar conclusion was reached by Dressler & Richstone (1990), who used an orbit-based code to infer the stellar kinematics in M87 assuming $M_h = 3.6 \times 10^9 M_\odot$.

Although our best estimates of $\beta(r)$ suggest a rapidly increasing anisotropy at small radii, the confidence bands on β become very wide at small r , and it is not obvious from Fig. 2 whether the central decline in β that we find using the two larger values of M_h is statistically significant. One way to address this question is to ask: What fraction of

the bootstrap estimates have a lower value of β at $0.5''$ (say) than at $2''$? We find that the decrease in β between $2''$ and $0.5''$ is significant at the 98% level for $M_h = 2.4$ and $3.8 \times 10^9 M_\odot$, and at the 43% level for $M_h = 1.0 \times 10^9 M_\odot$. If Ford et al. (1996) are correct in speculating that turbulent motions in the M87 gas disk might imply an even larger mass than $3.8 \times 10^9 M_\odot$, the central decline in $\beta(r)$ would become even more significant.

5. Discussion

Our conclusion that σ_r is approximately equal to, or slightly greater than, σ_t throughout the main body of M87 is unremarkable. However the apparent predominance of circular over radial motions at the very center of M87 is potentially more interesting. A number of models for the formation of nuclear black holes predict a bias toward circular motions within the radius of influence of the black hole, $r_h = GM_h/\sigma^2$, or $\sim 1''$ in M87. This is roughly the radius at which we find that σ_r must fall below σ_t when $M_h \geq 1.0 \times 10^9 M_\odot$. (As often noted, r_h in M87 is also roughly equal to the size of the seeing disk, a coincidence that is hopefully fortuitous!) Thus it seems appropriate to ask whether the anisotropy that we infer in the stellar motions could be a relic of the black hole formation process.

In one widely-discussed class of models, black holes grow from the accumulation of gas on a timescale long enough that the stellar action variables are adiabatically conserved. The gradual deepening of the gravitational potential in these models can induce a tangential anisotropy in the stellar motions at radii near r_h . Young (1980) first noticed this effect in numerical calculations, and Goodman & Binney (1984) showed that the adiabatic growth of a black hole at the center of an initially isothermal galaxy always enhances the tangential components of the velocity dispersion at the expense of the radial component. However the effect is subtle, since the eccentricities of orbits in axisymmetric systems are almost unaffected by slow changes in the potential (Lynden-Bell 1963). Quinlan, Hernquist & Sigurdsson (1995) followed the adiabatic growth of black holes in a variety of spherical, initially isotropic galaxy models, with and without constant-density cores. The resulting $\beta(r)$ profiles varied from model to model, but the value of β at $r = r_h$ was always close to its minimum, with β_{min} typically lying between -0.3 and 0 . Such mild anisotropies would be almost undetectable in M87 given the quality of data currently available.

Black holes might also grow by the capture of stars on low angular momentum orbits, whose pericenters lie within the tidal breakup radius r_t of the black hole (Hills 1975). One result would be to remove elongated orbits from the central regions of the galaxy and hence to increase the ratio of σ_t to σ_r (e.g. Cohn & Kulsrud 1978, Fig. 8). However the tidal radius of a $\sim 10^9 M_\odot$ black hole is comparable to its Schwarzschild radius, or $\sim 10^{-4}$ pc

in the case of the M87 black hole – much too small to be observed. Scattering of stars at larger radii into the loss cone (Frank & Rees 1976) would be unimportant due to the long relaxation time in M87.

In yet another class of models, nuclear black holes grow through the accretion of other black holes acquired from galaxy mergers (e.g. Ebisuzaki, Makino & Okumura 1991). Dynamical friction drags the black holes into the central region where they form a bound pair. The subsequent evolution was outlined by Begelman, Blandford & Rees (1990): the binary separation shrinks with time—at first through dynamical friction, later because of three-body scattering processes in which the hard binary ejects stars from the center—until it becomes small enough that gravitational radiation causes the black holes to merge. The mass of stars ejected by the binary can be comparable to the sum of the two black hole masses (Quinlan 1996). Because the binary interacts most strongly with stars on elongated orbits, three-body scattering should introduce a tangential bias in the velocity distribution of the remaining stars. Detailed simulations of this complicated process have yet to be published, but it seems plausible that the induced anisotropy could be much greater than in the adiabatic-growth or tidal-disruption models.

Although our conclusions about the stellar dynamics of M87 are qualitatively consistent with the predictions of all these models, we stress that the case for a massive black hole is not strengthened in any way by our work. The low, central value of the stellar velocity dispersion in M87 continues to be surprising given the independent evidence for a dark mass. If a massive black hole is indeed present in M87, then nature has somehow conspired to hide its effects on the stellar kinematics by adjusting the shapes of the stellar orbits. As discussed above, such a conspiracy is not impossible to imagine, but one would still like to find evidence in the stellar kinematics for the central singularity. The bias toward circular orbits that we infer at $\sim 1''$ is not sufficient to keep the observed dispersions low at arbitrarily small radii; eventually, even exactly circular motions would be expected to show a Keplerian rise. Observations of M87 with the Space Telescope Imaging Spectrograph (Baum et al. 1996) should allow accurate measurement of the stellar velocity dispersion at a radius of $0.2'' \approx 16$ pc, where the orbital velocity around a $2.4 \times 10^9 M_\odot$ black hole would be ~ 800 km s $^{-1}$. Such high velocities would leave their mark on the line-of-sight velocity dispersion profile regardless of the shapes of the stellar orbits.

We thank R. van der Marel for assisting in the data interpretation, and G. Quinlan for helping us to understand the various models for black hole formation. This work was supported by NSF grant AST 90-16515 and NASA grant NAG 5-2803 to DM.

Table 1: M87 Stellar Mass-To-Light Ratio

M_h/M_\odot	$(M/L)_I$	68%	95%
1.0×10^9	3.76	(2.94, 5.96)	(2.33, 9.44)
2.4×10^9	3.72	(2.89, 5.91)	(2.29, 9.39)
3.8×10^9	3.68	(2.86, 5.88)	(2.26, 9.31)

REFERENCES

- Baum, S. et al. 1996, STIS Instrument Handbook, Version 1.0 (Baltimore: STScI)
- Begelman, M. C., Blandford, R. D. & Rees, M. J. 1980, *Nature*, 287, 307
- Binney, J. J. & Mamon, G. A. 1982, *MNRAS*, 200, 361
- Cohn, H. & Kulsrud, R. M. 1978, *ApJ*, 226, 1087
- Dejonghe, H. & Merritt, D. 1992, *ApJ*, 391, 531
- Dressler, A. 1980, *ApJ*, 240, L11
- Dressler, A. & Richstone, D. O. 1990, *ApJ*, 348, 120
- Ebisuzaki, T., Makino J., & Okumura, S. K. 1991, *Nature*, 354 212
- Efron, B. 1982, *The Jackknife, the Bootstrap and Other Resampling Plans* (Philadelphia: SIAM)
- Ford, H. C., Harms, R. J., Tsvetanov, Z. I., Hartig, G. F., Dressel, L. L., Kriss, G. A., Bohlin, R. C., Davidsen, A. F., Margon, B. & Kochhar, A. K. 1994, *ApJ*, 435, L27
- Ford, H. C., Ferrarese, L., Hartig, G., Jaffe, W., Tsvetanov, Z. & van den Bosch, F. 1996, in *Nobel Symposium No. 98, Barred Galaxies and Circumnuclear Activity*, ed. A. Sandqvist & P. O. Lindblad (Heidelberg: Springer), 293
- Frank, J. & Rees, M. J. 1976, *MNRAS*, 176, 633
- Goodman, J. & Binney, J. J. 1984, *MNRAS*, 207, 511
- Harms, R. J., Ford, H. C., Tsvetanov, Z. I., Hartig, G. F., Dressel, L. L., Kriss, G. A., Bohlin, R. C., Davidsen, A. F., Margon, B. & Kochhar, A. K. 1994, *ApJ*, 435, L35
- Hills, J. G. 1975, *Nature*, 254, 295
- Jarvis, B. J. & Peletier, R. F. 1991, *AA*, 247, 315
- Kormendy, J. & Richstone, D. O. 1995, *ARAA*, 33
- Lauer, T. R. et al. 1992, *AJ*, 103, 703
- Lynden-Bell, D. 1963, *The Observatory*, No. 932, 23

- Merritt, D. 1987, *ApJ*, 319, 55
- Merritt, D. 1993a, in *Structure, Dynamics and Chemical Evolution of Elliptical Galaxies*, ed. I. J. Danziger, W. W. Zeilinger & K. Kj ar (Munich: ESO), 275
- Merritt, D. 1993b, *ApJ*, 413, 79
- O’Sullivan, F. 1986, *Statist. Sci.*, 1, 502
- Peletier, R. F., Davies, R. L., Illingworth, G. D., Davies, L. E. & Cawson, M. 1990, *AJ*, 100, 1091
- Qian, E. E., de Zeeuw, P. T., van der Marel, R. P. & Hunter, C. 1995, *MNRAS*, 274, 602
- Quinlan, G. D. 1996, *New Astronomy*, 1, 35
- Quinlan, G. D., Hernquist, L. & Sigurdsson, S. 1995, *ApJ*, 440, 554
- Richstone, D. O. & Tremaine, S. 1985, *ApJ*, 296, 370
- Sargent, W. L. W., Young, P. J., Boksenberg, A., Shortridge, K., Lynds, C. R. & Hartwick, F. D. A. 1978, *ApJ*, 221, 731.
- van der Marel, R. P. 1994, *MNRAS*, 270, 271
- Wahba, G. 1990, *Spline Models for Observational Data* (Philadelphia: SIAM)
- Young, P. 1980, *ApJ*, 242, 1232

Fig. 1.—

Line-of-sight velocity dispersions in M87. Open circles: G-band measurements from van der Marel (1994). The innermost data point has been shifted from its true position at $R = 0''$. Solid line: velocity dispersion profile corrected for the effects of seeing and instrumental blurring. Dashed lines: 90%, 95% and 99% confidence bands on the corrected profile.

Fig. 2.—

Velocity dispersions and anisotropy as a function of radius in M87, for three different values of the black hole mass: $M_h = 1.0 \times 10^9 M_\odot$ (a), $2.4 \times 10^9 M_\odot$ (b) and $3.8 \times 10^9 M_\odot$ (c). Left hand column: radial (heavy curves) and transverse (thin curves) velocity dispersions; dashed curves are 95% confidence bands. Right hand column: velocity anisotropy, $\beta = 1 - \sigma_t^2/\sigma_r^2$, with 95% confidence bands.

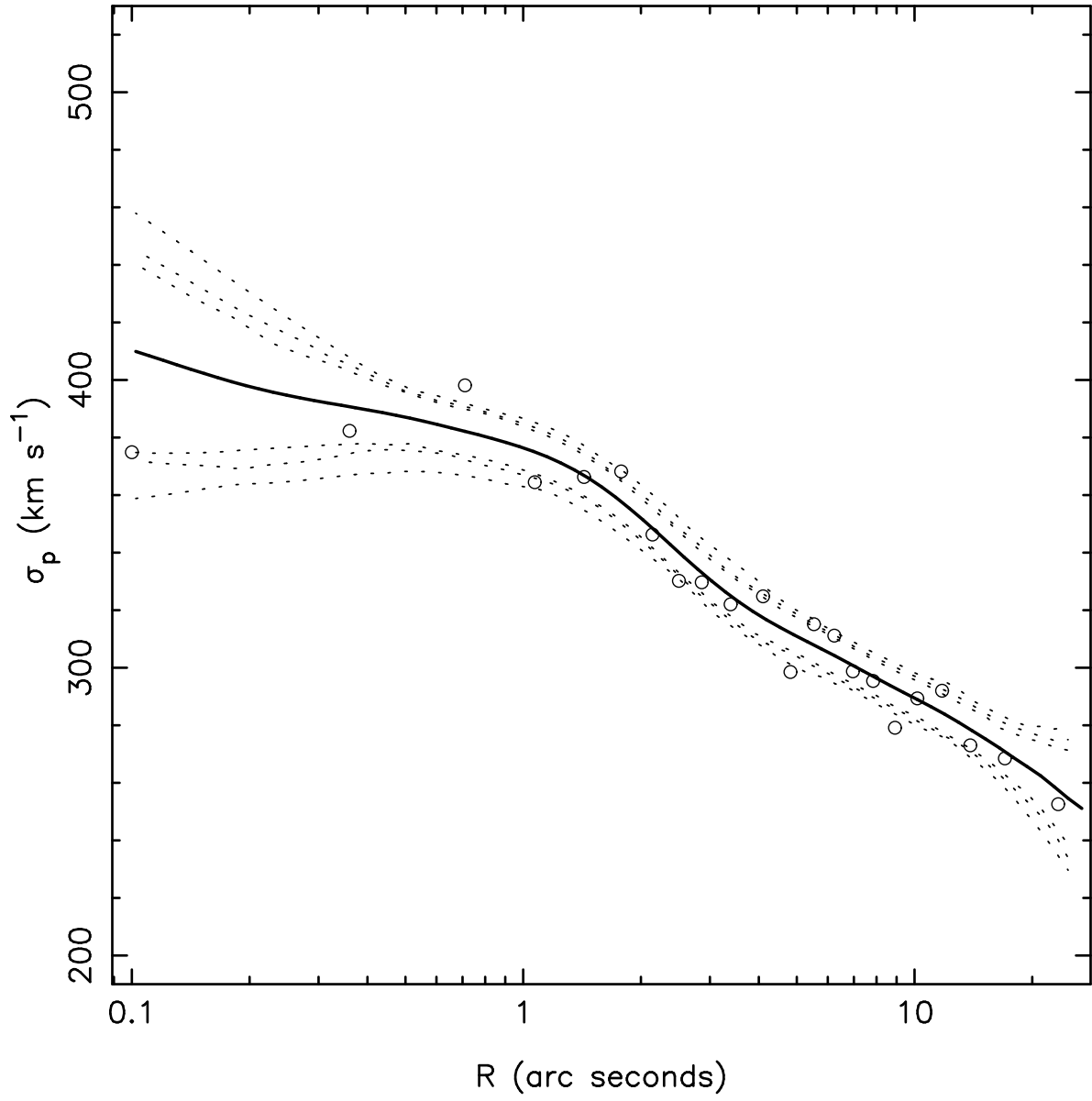


Fig. 1.—

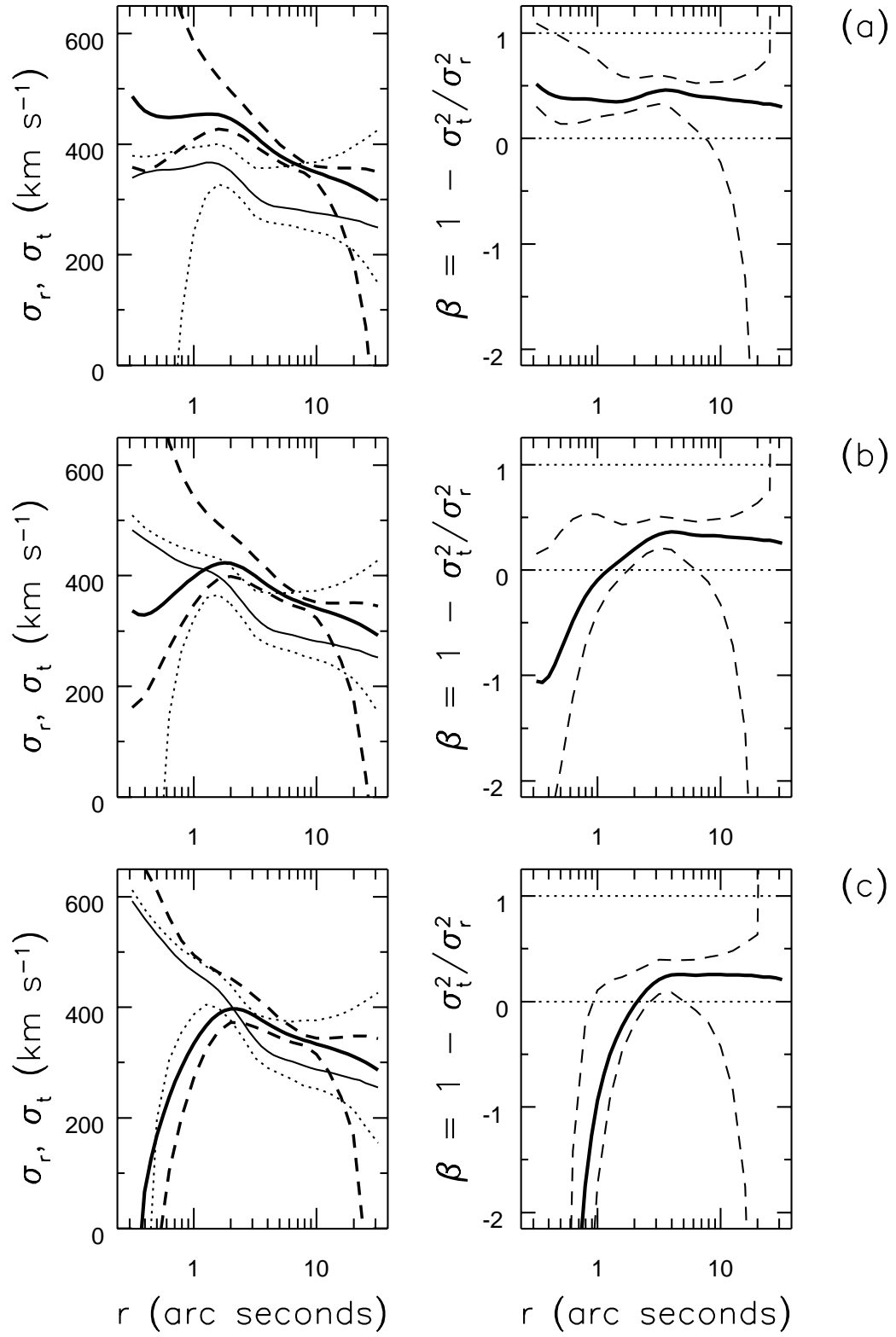


Fig. 2.—